Charge-transfer and impulsive electronic-to-vibrational energy conversion in ferricyanide: ultrafast photoelectron and transient infrared studies

Ojeda, José ; Arrell, Christopher A ; Longetti, Luca ; Chergui, Majed ; Helbing, Jan

Abstract: The photophysics of ferricyanide in H2O, D2O and ethylene glycol was studied upon excitation of ligand-to-metal charge transfer (LMCT) transitions by combining ultrafast photoelectron spectroscopy (PES) of liquids and transient vibrational spectroscopy. Upon 400 nm excitation in water, the PES results show a prompt reduction of the Fe 3+ to Fe 2+ and a back electron transfer in 0.5 ps concomitant with the appearance and decay of a strongly broadened infrared absorption at 2065 cm -1 . In ethylene glycol, the same IR absorption band decays in 1 ps, implying a strong dependence of the back electron transfer on the solvent. Thereafter, the ground state ferric species is left vibrationally hot with significant excitation of up to two quanta of the CN-stretch modes, which completely decay on a 10 ps time scale. Under 265 nm excitation even higher CN-stretch levels are populated. Finally, from a tiny residual transient IR signal, we deduce that less than 2% of the excited species undergo photoaquation, in line with early flash photolysis experiments. The latter is more significant at 265 nm compared to 400 nm excitation, which suggests photodissociation in this system is an unlikely statistical process related to the large excess of vibrational energy.

DOI: https://doi.org/10.1039/c7cp03337k

PCCP

Accepted Manuscript

ROYAL SOCIETY OF CHEMISTRY

rsc.li/pccp

View Article Online
DOI: 10.1039/C7CP03337K

Journal Name

ARTICLE TYPE

Cite this: DOI: 10.1039/xxxxxxxxxx

Charge-transfer and impusive electronic-to-vibrational energy conversion in ferricyanide: ultrafast photoelectron and transient infrared studies

José Ojeda,[a] Christopher A. Arrell,[a] Luca Longetti,[a] Majed Chergui,[a] and Jan Helbing[b]

Received Date
Accepted Date

DOI: 10.1039/xxxxxxxxxx

www.rsc.org/journalname

The photophysics of ferricyanide in H_2O, D_2O and ethylene glycol was studied upon excitation of ligand-to-metal charge transfer (LMCT) transitions by combining ultrafast photoelectron spectroscopy (PES) of liquids and transient vibrational spectroscopy. Upon 400 nm excitation in water, the PES results show a prompt reduction of the Fe^{3+} to Fe^{2+} and a back electron transfer in $\sim$ 0.5 ps concomitant with the appearance and decay of a strongly broadened infrared absorption at $\sim$ 2065 cm^{-1}. In ethylene glycol, the same IR absorption band decays in $\sim$ 1 ps, implying a strong dependence of the back electron transfer on the solvent. Thereafter, the ground state ferric species is left vibrationally hot with significant excitation of up to two quanta of the CN-stretch modes, which completely decay on a 10 ps time scale. Under 265 nm excitation even higher CN-stretch levels are populated. Finally, from a tiny residual transient IR signal, we deduce that less than 2 % of the excited species undergo photoaquation, in line with early flash photolysis experiments. The latter is more significant at 265 nm compared to 400 nm excitation, which suggests photodissociation in this system is an unlikely statistical process related to the large excess of vibrational energy.

1 Introduction

The study of intramolecular charge transfer processes in transition metal complexes is motivated by their numerous potential applications in fields ranging from electrochemistry, catalysis, photochemical energy conversion and magnetic devices to environmental chemistry. Although these systems have extensively been studied, their complex photophysics and photochemistry is still an active subject of research[1]. Iron hexacyanides are archetypal models for understanding charge transfer reactions in solution, where solvent effects play a significant role. Both $[Fe(CN)_6]^{3-}$ and $[Fe(CN)_6]^{4-}$ have octahedral (O_h) symmetry, but important differences arise due to the higher oxidation state of the ferric center and its vacancy in the ligand-field induced low-spin t_{2g} level. As an example, while the ferrous species has a charge transfer to solvent (CTTS) band in the UV-VIS spectral region[2,3], this transition is not observed for the ferric complex. Whereas the behavior of ferrocyanide under photo excitation is starting to be understood (there is a marked wavelength dependence of the branching ratio of photo aquation vs photo oxidation)[4–7], several questions remain open regarding the photochemistry of ferricyanide. Its relaxation pathways following photo excitation of a ligand-to-metal charge transfer (LMCT) transition have not been fully determined yet. Early work pointed to a complicated relaxation mechanism[4,5,8,9] in which neither the primary and secondary photo products nor the role of solvent interactions are clear.

The first ultrafast studies on solvated ferricyanide were conducted only recently. In an X-ray experiment with tens of ps temporal resolution, the creation of the aquated complex $[Fe(CN)_5OH_2]^{2-}$ was reported after excitation of aqueous ferricyanide at 355 nm.[6] However, this wavelength is poorly absorbed

[a] Laboratory of Ultrafast Spectroscopy, ISIC, and Lausanne Centre for Ultrafast Science (LACUS), Ecole Polytechnique Fédérale de Lausanne, CH-1015 Lausanne, Switzerland. E-mail: majed.chergui@epfl.ch
[b] University of Zurich, Department of Chemistry, Winterthurerstrasse 190, CH-8057 Zürich, Switzerland. E-mail: jan.helbing@chem.uzh.ch

† Electronic Supplementary Information (ESI) available: Linear absorption spectra, decay-associated spectra, pump-power dependence. See DOI: 10.1039/b000000x/

View Article Online
DOI: 10.1039/C7CP03337K

as it lies roughly between two d-d forbidden transitions at $\sim$ 341 and 372 nm[10–12] and away from the allowed LMCT bands centered at $\sim$ 300 and $\sim$ 420 nm[13]. Excitation at 266 nm of another LMCT band[10,11,13] did not yield the same product. As pointed out by the authors, the findings in this study must be interpreted with caution because the $\sim$ 10 ps duration of the pump pulse could also lead to re-excitation of intermediate transient states or species.

In the sub-picosecond regime, the temporal evolution of the CN-stretch band of ferricyanide in acetonitrile (MeCN) and dimethyl sulfoxide (DMSO) was probed by IR transient absorption.[14] Very precise anisotropy measurements revealed that the O_h symmetry of the complex is conserved during LMCT photo excitation at $\sim$ 400 nm. Two solvent-dependent time constants were associated to the subsequent localization of the ligand hole, followed by metal to ligand back transfer during excited state decay. However, the assignment of transient bands in the 2080-2100 cm^{-1} region to a Fe^{2+} molecule in that study is difficult to reconcile with earlier findings that the CN-stretch vibrations of ferrous complexes lie usually very close to that of ferrocyanide (2039 cm^{-1})[15]. We found it also surprising that symmetry breaking (by hole localization) in a $Fe(CN)_6$ complex can be sufficient to cause the splitting of a triply degenerate CN-stretch mode into two strong bands separated by approximately 20 cm^{-1}. More recently, $[Fe(CN)_6]^{3-}$ dissolved in formamide has also served as a model system for two-dimensional vibrational-electronic spectroscopy[16], showing now strong dependence of the IR-response on excitation energy within the 400 nm LMCT band.

In order to clarify the processes induced by LMCT excitation in water-solvated ferricyanide, we perform here a study combining ultrafast photoelectron spectroscopy (PES) and IR transient absorption (TA) spectroscopy. In both cases, the $^2T_{2g} \rightarrow {}^2T_{1u}(t_{1u} \rightarrow t_{2g})$ band (centered at $\sim$ 420 nm) is excited at $\sim$ 395 nm. The 25$^{\text{th}}$ harmonic ($\sim$ 39 eV) of the fundamental 800 nm pulse is used for recording the photoelectron spectrum, while the polarization-resolved transient IR experiment probes the CN-stretch region of the vibrational spectrum between $\sim$ 1950 - 2180 cm^{-1}. We complement these studies by IR measurements upon excitation of a higher-lying LMCT state at 266 nm and explore solvent-dependent effects in D_2O and ethylene glycol (Etgly).

Ultrafast PES of solutions is an emerging technique[17–23] that is increasingly being implemented with success for studying ultrafast dynamics of solvated transition metal complexes[23,24]. PES is ideal for directly tracking the oxidation state changes of an atomic or molecular species by measuring its binding energy (BE). In the present case, it provides distinct signatures of Fe^{2+} and Fe^{3+} cyanides due to their different ligand fields, e.g., their t_{2g} highest occupied molecular orbital (HOMO) is $\sim$ 1.4 eV apart for aqueous hexacyanides in a region where neither ligand nor solvent contributions are present.[25] At short time delays, PES often allows for a more immediate interpretation than transient absorption spectra as there is no need to disentangle overlapping contributions from excited state absorption, ground state bleach and stimulated emission. Nevertheless, a few ps after photo excitation, effects such as space charge[26] and solvent heating[27] can be difficult to separate from the transient signal.

Transient IR spectroscopy provides a unique probe of the symmetry of the complex and the ligand vibrations are very sensitive to the oxidation state of a central metal atom. Only the triply-degenerate T_{1u} CN-stretch mode is IR-active in the octahedral hexacyanides. Its oscillator strength is about four times smaller for the ferric $[Fe(CN)_6]^{3-}$ than for the ferrous $[Fe(CN)_6]^{4-}$ ion, for which it is also red-shifted by approximately 80 cm^{-1}.[28] In the present work, PES is used to clearly track the LMCT process and its lifetime, which are then used to identify the IR features of the reduced Fe^{2+} species. The IR data allow us to fully map out the subsequent relaxation kinetics following LMCT excitation and to identify the Fe(II) penta-aquo photochemical product.

2 Experimental methods

Potassium ferricyanide was purchased from Sigma Aldrich (purity $\geq$ 99%, contaminating iron compounds < 0.05%) and used as received. MilliQ water (18.2 MΩ·cm) from a Millipore machine was used for preparing the aqueous solutions. As ferricyanide can undergo photo degradation, samples were freshly prepared before the measurements. Upon addition of the solute, they were sonicated to ensure homogeneous mixing and subsequently filtered with 2 μm pore size Millipore paper. While highly concentrated solutions ($\sim$ 700 mM) were used for the PES experiment, concentrations of 50 mM or lower were used for the TA studies.

2.1 Photoelectron spectroscopy

A detailed description of the experimental setup can be found elsewhere[29,30]. Briefly, a tunable repetition rate (3-15 kHz) Ti:Sapphire laser is set to operate at 6 kHz and $\sim$ 1.5 mJ pulse energy, with a pulse duration of $\sim$ 40 fs at a central frequency of $\sim$ 790 nm. About 80 % of the laser energy is directed to a high-harmonic generation (HHG) chamber where the 25$^{\text{th}}$ harmonic ($\sim$ 39 eV) of the fundamental is generated in a continuous-flow Ar target and subsequently monochromatized with a single-grating EUV monochromator. The $\sim$ 0.8 eV, 45 fs EUV pulses are focused on the target (a $\sim$ 15 μm diameter liquid jet) into a sub-30 μm spot. The EUV probe polarization is kept parallel to the electron spectrometer detection axis and perpendicular to the liquid jet propagation direction.

For the optical pump line, the remaining pulse energy is loosely focused onto a BBO crystal to generate the $\sim$ 395 nm second harmonic of the fundamental radiation. The remaining IR is filtered by means of dielectric mirrors before reaching the target. The much reduced probe volume in PES compared to TA techniques

View Article Online
DOI: 10.1039/C7CP03337K

typically requires exciting a larger proportion of molecules. A pump energy of $\sim$ 5 μJ/pulse (fluence $\sim$ 16 mJ/cm^2) is chosen, which is significantly higher than the $\sim$ 0.5 μJ/pulse ($\sim$ 3 mJ/cm^2) excitation energy in the IR TA experiments but still within the linear excitation regime, as experimentally verified.

The laser-assisted photoelectric effect (LAPE)[31] is used to find the zero time delay between pump and probe, which gives a $\sim$ 80 fs temporal resolution. Four experimental runs were recorded under the same conditions for ensuring reproducibility.

The high concentration of the sample (0.7 M, lower than the $\sim$ 0.91 M saturation concentration[32] to prevent aggregation) in the PES measurements is due to the $\leq$ 2 nm electron probe depth at our EUV photon energy[33]. The first hydration shell of ferricyanide in water is about 4.8 Å, with 11 water molecules per ferricyanide ion.[34] At 0.7 M concentration, there are close to 79 water molecules per iron complex, thus ion-ion interactions should be negligible. The liquid jet flow rate is set at 0.35 ml/min (33 m/s). Within the $\sim$ 166 μs laser period the jet travels a distance of $\sim$ 5.5 mm, so that every laser pulse finds a refreshed sample surface.

2.2 Transient IR absorption

The sample was circulated in a home-build flow cell, which consisted of two 2 mm-thick CaF_2 windows separated by a 50 μm PTFE spacer. The laser beams were focused onto a narrow channel where the flow speed was sufficiently high to ensure complete exchange of sample between two consecutive shots. A larger opening served for linear absorption measurements in a UV-VIS and an FTIR spectrometer. In water and D_2O the optical density of both the LMCT band at 400 nm and the CN-stretch transition at $\sim$ 2115 cm^{-1} was close to 0.25, while in Etgly the absorbance was more than 10 times smaller due to reduced solubility.

UV pump pulses centered at $\sim$ 395 nm or $\sim$ 265 nm (frequency doubling and tripling) and mid-IR probe pulses (OPA followed by difference-frequency mixing) were generated from an amplified femtosecond laser system producing $\sim$ 100 fs pulses at $\sim$ 790 nm with a repetition rate of 1 kHz. The mid-IR light was split into a reference beam and a probe beam, which was overlapped with the UV-pump in the sample (focal diameters $\sim$ 80 μm IR, 150 μm UV). Probe and reference were dispersed in a spectrometer and recorded simultaneously by a double array (2x32 pixel) MCT detector. For low resolution measurements (7 cm^{-1}) a 150 l/mm grating was used. Much higher resolution (3 cm^{-1}) was achieved with a 300 l/mm grating, which was repeatedly rotated between two positions during the transient scans in order to cover the $\sim$ 2010-2130 cm^{-1} spectral range. The low resolution measurement was used to correct for different baseline offsets in the two high resolution data sets.

The energy of the excitation light was kept at $\sim$ 0.5 μJ/pulse (3 mJ/cm^2) to avoid damage to the cell windows. A polarizer, followed by a motorized half-wave plate in the pump beam allowed us to measure signals with parallel and perpendicular polarization quasi simultaneously. From these signals the magic angle response and the anisotropy were calculated.

The $\sim$ 180 fs temporal resolution of the setup was determined by recording the transmission change of a silicon wafer placed behind a 2 mm CaF_2 window at the sample position. However, the signal near zero time delay is also influenced by cross-phase modulation in the solvent and the cell windows, which was found to contribute significantly for delays between -200 fs and 200 fs. The cross phase modulation signal was recorded independently by repeating the scan with pure solvent and subsequently subtracted.

3 Results

3.1 Photoelectron spectroscopy

The inset of Fig. 1 shows the static PES spectra of aqueous $K_4[Fe(CN)_6]$ and $K_3[Fe(CN)_6]$ solutions in the region of the HOMO of $Fe^{2+/3+}$. The band at 11.16 eV is due to the water solution HOMO band to which both spectra are normalized. As already mentioned, the clear separation of the bands at $\sim$ 6.1 and 7.5 eV BE makes PES ideal for determining the oxidation state of the metal center.

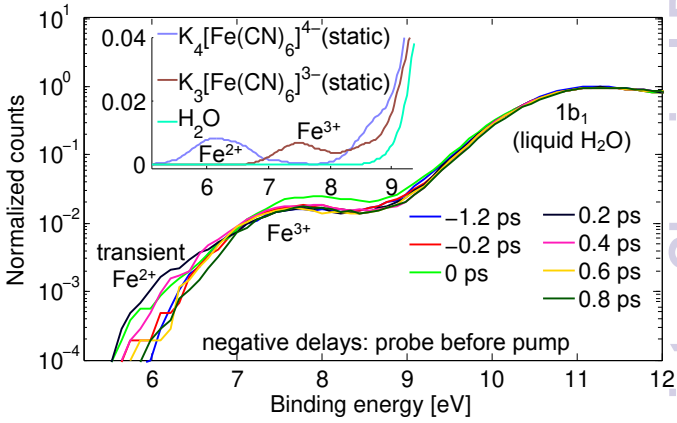

Fig. 1 Time-resolved photoelectron spectra of aqueous ferricyanide upon photo excitation of the LMCT band centered at $\sim$ 420 nm. The inset shows the static (unpumped) photoelectron spectra of water and aqueous ferro- and ferricyanide solutions in the region of the $Fe^{2+/3+}$ HOMO. The oxidation state of the iron center is easily distinguishable[25]

The main figure shows a set of pump-probe photoelectron spectra of a $\sim$ 700 mM aqueous ferricyanide solution upon excitation at $\sim$ 395 nm. There is a transient signal around the 6.1 eV BE region that appears at zero time delay (i.e., within the time resolution of our experiment) and then rapidly decays within a few hundred femtoseconds. This is evidence of impulsive photo reduction of the iron, in line with the LMCT character of the transi-

View Article Online
DOI: 10.1039/C7CP03337K

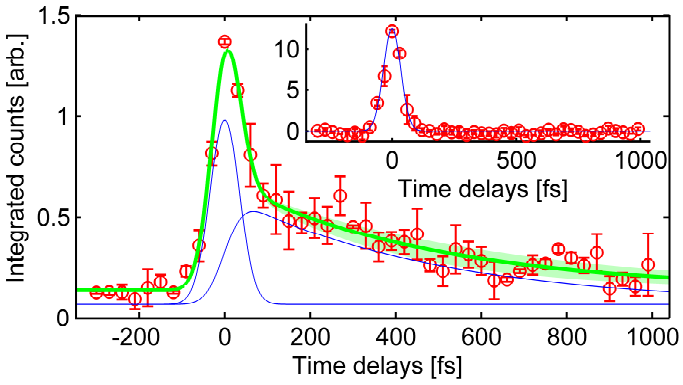

Fig. 2 Integrated raw photoelectron counts from photoelectron spectra (red circles) normalized to the intensity of the water HOMO band. Inset: in a binding energy window (7.15 to 7.85 eV) corresponding to the Fe^{3+} HOMO of the unpumped molecules, where the cross-correlation signal is evident. Main figure: in a BE window (5.7 to 6.5 eV) containing the Fe^{2+} transient signal, which decays with a time constant of 475 ± 130 fs. Error bars represent the standard deviation over several experimental runs.

tion.

The integrated photoelectron counts in the Fe^{3+} region (∼ 7.15 to 7.85 eV) are depicted in the inset of Fig. 2. Since it entails a tiny change relative to the background, the impulsive decrease in ferricyanide photoelectron counts is not obvious. The symmetric signal around zero time delay is due to a redistribution of photoelectron counts to sidebands at zero time delay, resulting from the LAPE[31], which provides a cross-correlation of pump and probe pulses of ∼ 80 fs FWHM.

The main figure shows the time evolution of the Fe^{2+} transient, integrated in the 5.7 to 6.5 eV binding energy window. The thin blue Gaussian around zero time delay represents the scaled LAPE contribution (from the inset), while the second thin blue trace corresponds to the fit of the error function convoluted with a single exponential decay. Both blue components contain a small baseline contribution as determined from the fit. The thick green curve is the sum of the LAPE and Fe^{2+} transients and decays with a time constant of 475 ± 130 fs. The shaded region represents the 95 % confidence bounds of the fit.

The PES data clearly shows that the iron center is impulsively reduced upon LMCT photo excitation and that it decays in the order of 0.5 ps. This decay reflects the back electron transfer, whose signature is also seen in the IR data below. Within the experimental signal-to-noise level, limited by the small probed volume and the low percentage of photo excited species in solution, no further changes are observed.

3.2 Transient IR absorption

As already mentioned the only IR-allowed band of $[Fe(CN)_6]^{3-}$ in the spectral window of interest is due to the triply-degenerate (T_{1u}) CN-stretch mode. In H_2O it is found at 2115.5 cm^{-1} with a width of approximately 10 cm^{-1}. In Etgly it is slightly red shifted and significantly broader (2113 cm^{-1} with FWHM ≈ 15 cm^{-1}) due to solvent dielectric effects[35].

In H_2O, D_2O and Etgly, excitation at 395 nm leads to an immediate bleach of the CN-stretch band and gives rise to a red-shifted, broad absorption band, which is centered near 2065 cm^{-1} (Fig. 3). It decays on a sub-picosecond timescale in H_2O and D_2O. In these solvents we also observe an additional shoulder on the low-frequency side of the bleach (∼ 2105 cm^{-1}), which disappears within the first two picoseconds alongside a significant reduction of the initial bleach. Five picoseconds after excitation the transient spectra in H_2O and D_2O consist mainly of the reduced bleach at 2115 cm^{-1} and a similarly narrow positive absorption at 2093 cm^{-1}. They decay on the same time scale of 10 ps, leaving only a strongly tilted baseline (discussed below), which has been subtracted from the data shown in Fig. 3. In addition we observe a very small residual bleach at 2115 cm^{-1} and a tiny positive peak at 2048 cm^{-1} (see inset of Fig. 4). The transient spectra in Etgly are similar to those in water, but the decay of the broad absorption band is markedly slower, and the band widths of the bleach and the positive absorption band near 2090 cm^{-1} are larger. Signal-to-noise is not sufficient to distinguish any residual signals at the longest delays (100 ps).

An unrestricted global analysis of the data yields three dominant time constants in the order of ∼ 0.5 ps, 1 ps and 10 ps for H_2O and D_2O, which are compared in table 1. In Etgly, only two time constants are retrieved. Because of correlation between the fitted time constants we estimate their error to be of the order of 10-20%. For all three solvents, the first time constant (τ_1) is associated to the decay of the broad absorption band at 2065 cm^{-1} (see the supporting information for the decay-associated spectra). It is twice as long in Etgly than in H_2O and D_2O. The signal anisotropy is zero at all frequencies and at all delays within experimental error, as previously reported by Gaffney and coworkers for acetonitrile and DMSO[14].

The tilted baseline in water can be quantitatively accounted for by the heating of the solvent due to the energy dissipated by the solute. Indeed, the inset of Fig. 4 compares the 100 ps spectrum (circles) to the difference of the IR absorption of water at 30°C and 22°C (black trace). A Fourier filter was applied to the latter to suppress the oscillatory signal caused by an etalon effect in the sample cell and yielded the red line. The curves agree very well, revealing a marked drop in H_2O absorption on the high energy side of our spectral window and an increase at the low energy side. From the temperature difference of the FTIR spectra and the scaling factor needed to overlay the transient data, we deduce an

View Article Online
DOI: 10.1039/C7CP03337K

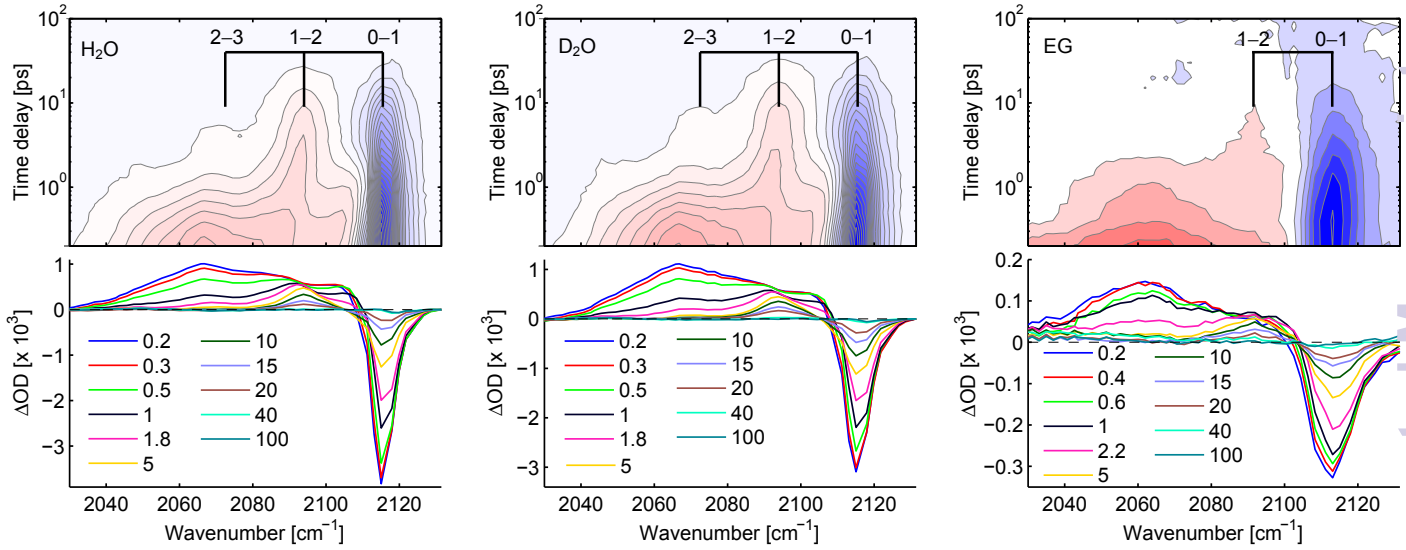

Fig. 3 Transient IR spectra of $[Fe(CN)_6]^{3-}$ excited at 400 nm, after subtraction of cross-phase modulation signal and solvent absorption changes. Left: H_2O, center: D_2O, right: ethylene glycol. The spacings of the grids in the 2D representations corresponds to the anharmonicity of the T_{1u} CN-strech mode in the electronic ground state.

Table 1 Time constants in ps from a global analysis of the transient IR data upon 400 nm excitation; τ_{IR} are the dominant decay constant after direct mid-IR excitation of the T_{1u} mode reported in the literature.

solvent	τ_1	τ_2	τ_3	τ_{IR} (ref)
H_2O	0.5	1.1	10	7.0 ± 1 (Sando *et al.*[36])
				7.3 ± 0.2 (Yu *et al.*[37])
D_2O	0.6	1.0	13	8.0 ± 1.5 (Sando *et al.*[36])
				8.1 ± 0.4 (Yu *et al.*[37])
				9.7 ± 1 (El Khoury *et al.*[28])
Etgly	1.2	–	9	8.5 ± 1.5 (Sando *et al.*[36])

increase in solvent temperature $\Delta T \approx 60$ mK, 100 ps after laser excitation. This is in good agreement with an estimate based on absorbed pump-laser power and excited sample volume. We have subtracted the heat signal of water from the transient data at all delays by scaling the red line in the inset of Fig. 4, to match the transient data at the low and high energy sides of our spectral window (≤ 1980 cm^{-1} and ≥ 2150 cm^{-1}), where no solute signal is seen. The amplitude of this baseline fit and the corresponding rise in H_2O temperature are plotted in Fig. 4 for two different data sets upon excitation at 400 nm and 266 nm.

The rise in solvent temperature can be fitted by a bi-exponential function

$$\Delta T(t) = a_1(1 - e^{-\frac{t-t_0}{\tau_1}}) + a_2(1 - e^{-\frac{t-t_0}{\tau_2}}) \quad (1)$$

shown by the thick solid lines in Fig. 4. A satisfactory fit required a delayed onset ($t_0 \approx 200 - 350$ fs) and two time constants $\tau_1 = 1 - 2$ ps and $\tau_2 = 7 - 10$ ps, with relatively large uncertainties due to

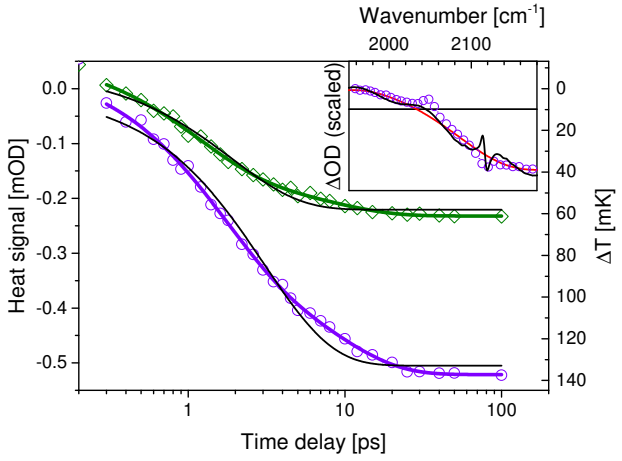

Fig. 4 Amplitude (at ~2160 cm^{-1}) of the baseline due to the temperature rise in H_2O for excitation at 400 nm (green diamonds) and 266 nm (purple circles). The right hand scale indicates the corresponding rise in solvent temperature. Thin black lines: single exponential fits, thick lines: bi-exponential fits. The inset shows the 100 ps transient spectrum for 266 nm excitation (circles) and the fitted baseline (red), which is the scaled FTIR temperature difference spectrum (black) after Fourier-filtering.

View Article Online
DOI: 10.1039/C7CP03337K

the strong interdependence of these parameters. A single time constant ($a_2 = 0$, $\tau_1 \approx 2$ ps) yielded only poor agreement with the data (thin black lines in Fig. 4). The ratio of the two amplitudes a_1/a_2 is also strongly dependent on the other fit parameters and on the order of 3-10. Despite these rather large uncertainties, the data clearly shows that heat dissipation to the solvent takes place on two distinct timescales, which are close to the τ_2 and τ_3 values in table 1.

A comparison of the background-corrected transient IR data for 400 nm and 266 nm excitation in H_2O is shown in Fig. 5. The amplitudes have been carefully scaled based on the observed temperature rise in H_2O and the difference in pump-photon energy to correspond to identical numbers of absorbed photons. In both cases we observe an immediate bleach of the T_{1u} CN-stretch band at 2115 cm^{-1} and a broad, red-shifted induced absorption. However, at the earliest measured time delays the bleach per absorbed photon is only approximately half as large upon 266 nm excitation but then decreases much more slowly. In addition, the short-lived induced broad absorption band centered at 2065 cm^{-1} seen immediately after 400 nm excitation in Fig. 5a is absent, or much weaker upon 266 nm excitation in Fig. 5b. The band at 2093 cm^{-1} reaches its maximum intensity only 7-8 ps after the 266 nm pump-pulses, while it is initially much stronger after 400 nm excitation. A shorter-lived induced absorption band centered at 2072 cm^{-1} is more pronounced after deep UV-excitation and we also observe two additional equally spaced bands further to the red in Fig. 5b. On the other hand, for delays longer than 8-10 ps the signals are largely identical and the positive band at 2093 cm^{-1} and the negative signal at 2115 cm^{-1} decay on the same 10 ps time scale, independent of excitation wavelength.

For better clarity, both Figs. 5a and 5b show data after subtraction of the 100 ps transient spectra, shown in Fig. 6 in the next section. At both excitation wavelengths these subtracted difference spectra show a small positive band at 2048 cm^{-1}, together with a tiny bleach contribution at 2115 cm^{-1} that amounts to less than 2 % of the initial bleach after 400 nm excitation.

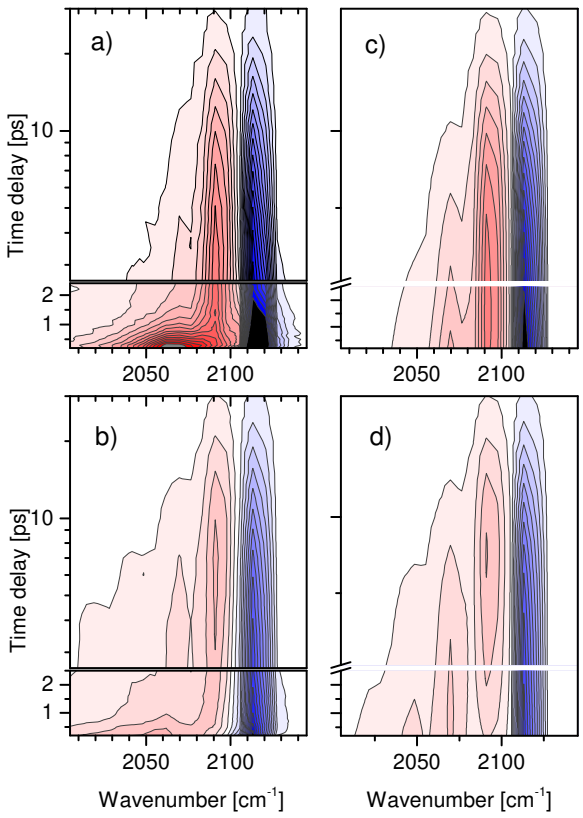

Fig. 5 Comparison of the transient IR spectra of $[Fe(CN)_6]^{3-}$ in H_2O after (a) 400 nm excitation and (b) 265 nm excitation. The intensity was scaled with the help of the solvent heat signal to represent equal numbers of absorbed photons. The time axis is linear before the break and logarithmic afterwards. (c) and (d) are fits using a sequential rate model for vibrational relaxation of a Poisson-distributed population. Only delays above the break line have been used for fitting after subtraction of the 100 ps signal from the experimental data.

4 Discussion

4.1 Band assignment

Table 2 summarizes the bands observed in the IR transient data upon 265 and 400 nm excitation. Their assignment, already partially discussed in the previous section, is detailed below.

In $[Fe(CN)_6]^{3-}$, the electronic transition near 400 nm is known as a LMCT transfer band, implying the transfer of an electron from the ligands to the Fe^{3+} core. The ferrous $[Fe(CN)_6]^{4-}$ ion has its T_{1u} absorption band at 2039 cm^{-1}, much narrower and further to the red than the short-lived band at 2065 cm^{-1}, which we observe immediately after 400 nm excitation. However, this discrepancy can be explained by the fact that the charge of the whole molecule is not altered by the absorption of a 400 nm pho-

View Article Online
DOI: 10.1039/C7CP03337K

Table 2 Observed bands in the transient IR data (in cm^{-1}) and their assignments. ESA: CN-stretch in the electronically excited (reduced) state. v = 0–1: Fundamental transition, and v = n–n+1: transition between higher vibrational levels of the T_{1u} CN-stretch mode of ferricyanide in the electronic ground state. an. shift.: anharmonically shifted fundamental.

solvent/excitation	ESA	v = 0–1	v = 1–2	v = 2–3	v = 3–4	an. shift
H_2O & D_2O/400 nm	2065	2115	2093	2072		2105 (shoulder)
Ethylene glycol/400 nm	2062	2113	2090			
H_2O/265 nm		2115	2093	2072	2050	

ton. Furthermore, 300 fs after excitation the surface under the excited state absorption signal is about twice as large as the bleach, in line with the strong difference in oscillator strength between the CN-stretch band of the ferric and the ferrous species. The 0.5 ps decay constants of the 2065 cm^{-1} band in H_2O and of the transient photoelectron signal clearly reflect a transient photoreduction of the iron and its decay back to the Fe^{3+} form. On the other hand, the full decay of the photoelectron signal implies that all spectral features observed in the mid-infrared after 1 ps are caused by ferric species in the electronic ground state.

The decay of the reduced excited state band at around 2065 cm^{-1} is significantly longer in Etgly (1.2 ps) than in H_2O and D_2O (0.5-0.7 ps). A similar band, with a solvent-dependent lifetime has also been observed for ferricyanide in DMSO and acetonitrile by Gaffney and coworkers [14], but its decay was assigned to hole localization on the ligands rather than re-oxidation of the iron.

At longer pump-probe delays our transient IR spectra in H_2O and D_2O very closely resemble the signals measured by Sando *et al.* [36], Yu *et al.* [37], as well as El Khoury *et al.* [28] after direct infrared excitation of the T_{1u} CN-stretch mode to the $v = 1$ level. In particular, the separation of the bleach signal at 2115 cm^{-1} and the positive band we observe at 2093 cm^{-1} corresponds exactly to the reported signal maxima (Fig. 3 in El Khoury *et al.* [28]). The dominant time constants in the (bi)-exponential decays after direct vibrational excitation (7-8 ps in H_2O, 8-10 ps in D_2O, $\sim$ 8.5 ps in Etgly, see table 1) are also very close to the slowest decay components after 400 nm excitation. This is strong evidence that the 2093 cm^{-1} band is due to the CN-stretch $v = 1 \rightarrow v = 2$ transition of the ground state molecule, and we can assign the band at 2072 cm^{-1} to the $v = 2 \rightarrow v = 3$ transition. In the data recorded with 265 nm excitation there is evidence of even higher vibrational excitation by the presence of a $v = 3 \rightarrow v = 4$ signal at 2050 cm^{-1}.

In their study of ferricyanide in DMSO and acetonitrile, Gaffney and coworkers reported an induced absorption band that is red-shifted by the same $\sim$ 22 cm^{-1} with respect to the bleach of the fundamental T_{1u} CN-stretch transition after 400 nm excitation [14]. However, they also observed a second band in between this band and the bleach signal, which appeared to decay on the same 10 ps timescale. As a result, they assigned both bands to fundamental ($v = 0 \rightarrow v = 1$) transitions of an ion with reduced symmetry. The weakly shifted band is also present in our data after 400 nm excitation in water, but it is only seen as a short-lived shoulder on the low energy side of the fundamental bleach near 2105 cm^{-1}. It has the typical signature of a fundamental transition that is red-shifted due to excitation of lower-lying vibrational states [38,39], which couple anharmonically to the high frequency mode. The low frequency modes are most likely excited during electronic relaxation, and the decay of the positive shoulder near 2105 cm^{-1} reflects the subsequent energy dissipation to the solvent. For the low frequency modes, this energy dissipation appears to be markedly faster in water (1-2 ps) than in DMSO or acetonitrile (5-10 ps) [14], while the high frequency CN-stretch excitations decay on a similar 10 ps time scale in all solvents. It is only slightly faster in H_2O than in D_2O in agreement with previous transient IR-IR studies [36] but the difference is rather small given the much higher density of states of H_2O in the CN-stretch region. Even more surprisingly, the CN-stretch modes decay almost equally fast in Etgly, although this solvent lacks vibrational transitions in this spectral region.

4.2 Electronic-to-vibrational energy transfer

In our data recorded in water, the solvent response provides independent evidence for energy dissipation on two distinct timescales. Indeed, the initial temperature rise in the solvent (Fig. 4) takes place in parallel with the disappearance of the 2105 cm^{-1} shoulder, while the time-constant of the second heating phase corresponds to the decay of the $v = 1$ level of the CN-stretch mode.

The decay of the LMCT excited state after 400 nm excitation seems to (re-)populate predominately the $v = 0$ level of the T_{1u} vibration in the electronic ground state, leading to the strong decrease of the negative signal at 2115 cm^{-1} within the first picosecond after excitation. Upon 265 nm excitation, on the other hand, the LMCT band at 2065 cm^{-1} is not observed, and the excited state decay appears to be instantaneous within the time-resolution of our IR experiment. The short-lived shoulder to the red of the fundamental transition is not seen either, but the initial red-shift of the $v = 1 \rightarrow v = 2$ band in Fig. 5b is a similar signature of anharmonic coupling to low-frequency modes in a hot ground state. The fact that the 2093 cm^{-1} band reaches its maximum intensity only 8 ps after 265 nm excitation indicates that levels

View Article Online
DOI: 10.1039/C7CP03337K

with $v \geq 1$ are populated significantly.

To quantify the amount of excitation in the CN-stretch modes, we have fitted the data for delays longer than 2.5 ps, when there are only minor contributions from band-shifts and band-narrowing due to cooling. Our model assumes an initial Poisson-distributed population of the vibrational levels and a sequential decay with fixed ratios of the rate constants (see appendix for details). It has essentially only two free parameters, the mean of the initial Poisson distribution and the $v = 1 \rightarrow v = 0$ rate constant. Nevertheless, Figs. 5c and 5d illustrate the excellent agreement between experimental and fitted spectra for both 400 nm and 265 nm excitation. The fits yield a $(8 \pm 1$ ps$)^{-1}$ rate for the $v = 1 \rightarrow v = 0$ decay, which is even closer to the time constants reported after direct IR excitation than the result of our global fit (see table 1). Our vibrational relaxation model also reproduces the delayed maximum of the 2093 cm^{-1} band (1-2 transition) after 8 ps under deep UV excitation. This is consequence of the decay of the $v = 2$ population and its stimulated emission contribution at that frequency[40]. The mean of the fitted Poisson distribution for 265 nm excitation is ~ 1.4, suggesting that of the molecules missing from the $v = 0$ ground state, roughly 50 % are promoted to the $v = 1$ level, 30 % to $v = 2$ and 15 % to $v = 3$. At 400 nm, the fitted mean is ~ 0.7 and the corresponding values are 75 %, 20 % and 5 %.

The excitation of one or even more quanta of the CN-stretch corresponds to a highly non-thermal vibrational energy population. It is unlikely caused by the (statistical) redistribution of excess energy in the molecule as it relaxes back to the electronic ground state. Rather, the strong excitation of this mode provides indirect evidence for an impulsive change in equilibrium Fe-C bond distance, which in turn can lead to an impulsive excitation of the CN-stretch vibration. The transient population of up to six quanta of a bridging CN-stretch mode has been reported by Khalil and coworkers as a result of ultrafast metal-to-metal (Fe^{2+}-Pt^{4+}) charge transfer in a complex where two ferrous $Fe(CN)_6$ units were linked via a CN-[$Pt^{4+}(NH_3)_4$]-NC bridge[41]. In that case charge was transferred in a well-defined direction across the bridging CN bond, whereas the LMCT transition of ferricyanide conserves the octahedral symmetry of the molecule, as evidenced by anisotropy data[14], and should affect all six ligands equally. A sudden radial kick would displace the $v = 0$ ground state vibrational wave function $\Psi_0(Q) \rightarrow \Psi_0(Q + \Delta Q)$, which can then be written in terms of the original basis:

$$\Psi_0(Q+\Delta Q) = \sum_{n=0}^{\infty} c_n \Psi_n(Q) \qquad (2)$$

For a harmonic oscillator, the square of the coefficients c_n follows a Poisson distribution:

$$|c_n|^2 = e^{-\mu} \frac{\mu^n}{n!}, \qquad (3)$$

where μ is the variance (and mean) of the distribution and increases quadratically with the displacement ΔQ. A value $\mu = 1.4$ as obtained from our fit of the 265 nm data corresponds to a displacement of approximately 0.06 Å of the ground state wavefunction. The energy thereby converted into vibrational excitation is only a small fraction (≤ 10 %) of the energy of the 265 nm pump pulse. This number is in good agreement with the weight of the slower time constant of the rise of solvent temperature in Fig. 4. The dominant contribution to the heat signal with a fast rise time thus seems to be due to the decay of the electronically excited (reduced) state, which is thus too fast to be resolved under 265 nm excitation. Indeed, electronic relaxation on extremely fast time scales is not uncommon in transition metal complexes[1,42].

We found that both the intensities of the CN-stretch bands and the heat signal in the solvent are strictly linear with pump-pulse energy. However, a vibrational wavepacket in the electronic ground state could also be created via a Raman process involving only two field interactions, which would follow the observed linear power dependence. As the bandwidth of our excitation pulses is much narrower than the CN-stretch frequency, this scenario would, however, also require significant impulsive motion along the CN-stretch coordinate in the electronically excited state, as well as a remarkably long electronic coherence lifetime.

Finally, we note that excitation of the T_{1u} mode need not be direct, but could also arise via the E_g and A_{1g} CN-stretch modes, which are only Raman-active and do not carry IR-oscillator strength in the octahedral complex. Excitation transfer from these dark modes to the IR-active T_{1u} mode probably accounts for the initial sub-picosecond decay components reported after direct mid-IR excitation[28]. Following electronic excitation, we expect equally fast equilibration within the $v = 1$ (or $v = 2$, $v = 3$, etc.) levels of the single, double and triply degenerate stretch vibrations. At very early delays, a non-equilibrated population of the E_g and A_{1g} CN-stretch modes could, however, contribute to the anharmonic shift of the T_{1u} transition, which produces the positive shoulder at 2105 cm^{-1} in our transient spectra in H_2O and D_2O.

During the submission process of this paper we became aware of work by Aziz and coworkers[43], who published PES data that is very similar to the transients shown in Fig. 2. The authors also report time-dependent DFT calculations which suggest significant Jahn-Teller distortions in the excited state manifold, associated with important changes to the equilibrium Fe-CN bond length. This may well be responsible for an impulsive excitation of the CN-stretch vibrations. On the other hand, we see no spectroscopic evidence for the intermediate electronic $^4B_{1g}$ state of reduced symmetry that was postulated in order to interpret a 170 fs component of the photoelectron transient in that work. This intermediary would imply a re-oxidation of the iron within 200 fs. Although this is at the limit of our time-resolution we would ex-

View Article Online
DOI: 10.1039/C7CP03337K

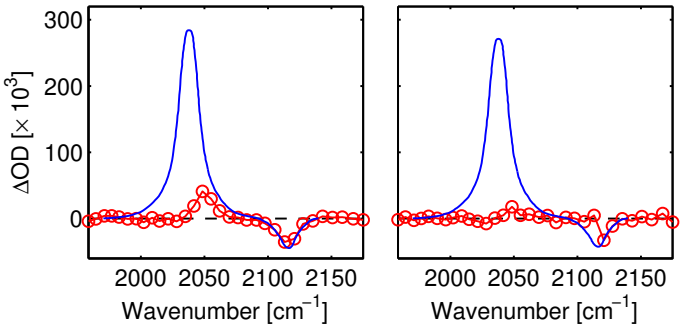

Fig. 6 Transient IR spectra (red circles) at 100 ps delay upon 265 nm (left) and 400 nm (right) excitation. The blue curve has been adapted from El Khoury *et al.*[28] and represents static spectra of ferro- and ferricyanide at identical concentrations. It has been scaled according to the observed bleach amplitude. A larger fraction of photoconverted species is evident upon 265 nm excitation.

pect to see at least a trace of such a change in the oxidation state in form of a fast spectral shift of the CN-stretch vibration. Furthermore, our assignment of the photoelectron transient, based on static experimental data (see inset of Fig. 1) indicates a 0.5 ps lifetime of the reduced iron. However, both studies report that the electronic decay is complete on a sub-picosecond timescale. Here we show that following this decay, multiple IR-bands simply reflect vibrational excitation in the ferric ground state. The predicted small Jahn-Teller-induced deviations from O_h symmetry in this ground state[43] are too weak to be observed experimentally and may actually be averaged out by fast solvent motion.

4.3 Photochemical reactions

Although we have shown in this work that the percentage of ferricyanide molecules undergoing permanent photoconversion upon LMCT excitation is very small, the tiny IR signal remaining at the longest time delay can serve to identify the nature of the final species.

Fig. 6 shows the transient spectra at long delay of ferricyanide in H_2O obtained upon 265 nm and 400 nm excitation, after correcting for solvent heating. The blue curves are static difference absorption spectra between ferro- and ferricyanide in D_2O (identical concentration of both species). They were adapted from the results of El Khoury *et al.*[28] by convolution with a 7.3 cm^{-1} FWHM Gaussian in order to account for the difference in spectral resolution and scaled to match the amplitude of the remaining bleach signal in our transient data at 100 ps delay.

There is significant difference between 265 nm and 400 nm excitation. In the former case, a positive signal appears at $\sim$ 2048 cm^{-1} and the remaining bleach band more closely resembles the width and position of the static CN-stretch in ferricyanide. Upon 400 nm excitation, the 2048 cm^{-1} band is much weaker and the bleach signal is apparently narrower and blue-shifted compared to the static CN-stretch. This signature resembles the signal obtained by heating the sample (see the black line in the inset of Fig. 4). Thus, under 265 nm excitation there must be a larger permanent bleach contribution and a higher proportion of molecules seem to undergo photoconversion.

It had been noted in early work that substitution of one CN ligand on iron hexacyanide molecules does not change the CN-stretch frequency significantly,[15] while a different oxidation state of the metal center entails a large shift of the CN-stretch band. This suggests that the 2048 cm^{-1} residual signal belongs to a photo-reduced molecule with a Fe^{2+} core. Indeed, other studies have identified reduced species as final products of ferricyanide photolysis[9].

The most likely species corresponding to our signal is the ferrous aquated ion $[Fe(CN)_5OH_2]^{3-}$, in which one cyanide ligand is replaced by a water molecule. Herington and Kynaston[15] found this molecule to absorb at 2043 $\pm$ 10 cm^{-1}. Furthermore, in a very recent investigation of the ultrafast photochemistry of ferrocyanide[7], a very similar product band near 2049 cm^{-1} was observed after 400 nm excitation, which was assigned to the ferrous photoaquated species. It is a known product of UV-vis irradiation of $[Fe(CN)_6]^{4-}$ in water and it is formed after the dissociation of a cyanide ion:

$$[Fe(CN)_6]^{4-} + H_2O \rightarrow [Fe(CN)_5OH_2]^{3-} + CN^- \quad (4)$$

For the same aquated molecule to form when starting from a ferric complex, the charge of the ion must be conserved, which implies the photodissociation of a cyanide radical:

$$[Fe(CN)_6]^{3-} + H_2O \rightarrow [Fe(CN)_5OH_2]^{3-} + CN\cdot \quad (5)$$

Such a scheme is compatible with the ligand-to-metal charge transfer character of the 400 nm and 265 nm excitation of the ferric complex. After the transfer of an electron to the iron core, radical dissociation would prevent its ultrafast re-oxidation, and the binding of a water molecule could stabilize the ferrous hexa-coordinated complex. We have, however, no direct spectroscopic evidence for this mechanism. The fundamental of the CN radical stretch vibration is expected near 2050 cm^{-1},[44] but its extinction coefficient is almost two orders of magnitude weaker than that of ferricyanide. As a result, CN radicals have not even been detected in transient IR experiments, even when they were produced with high quantum yield by photodissociation of ICN[45]. Due to the low efficiency of ferricyanide dissociation and spectral overlap with $Fe(CN)_6$ ions, it may also be difficult to identify the cyanide radicals in transient visible spectra, where they were shown to give rise to a rather broad band centred at 385 nm, shifting to shorter wavelengths during solvation[46].

Given the very small quantum yield of photo product formation, it is unlikely that ligand dissociation is a dominant reaction

View Article Online
DOI: 10.1039/C7CP03337K

channel (which would imply ultrafast geminate recombination of more than 98 % of the excited molecules). Rather we believe that CN radical dissociation is a statistical process associated with the large excess of vibrational energy in the system. Such a scenario would be consistent with our findings that both vibrational excitation and the photoproduct yield are higher after 265 nm compared to 400 nm excitation.

The tiny percentage of molecules undergoing long-term changes agrees with the very weak signals recently observed in a ps transient X-ray absorption study of ferricyanide[6]. In that work, no definite assignment of the photoproducts could be made under the assumption that they were only ferric species. Comparing the difference between the (experimental) X-ray absorption spectrum of the ferricyanide complex and the computed spectrum of the ferrous aquated pentacyanide molecule reported in that work, we can obtain a signal (not shown) that qualitatively matches the reported transient X-ray data 70 ps after 265 nm excitation.

Early flash photolysis experiments[8,9] have identified small concentrations of $[Fe(CN)_5OH_2]^{2-}$ and $[Fe(CN)_5OH]^{3-}$ as additional photo products of LMCT excitation of ferricyanide in water, but it is not entirely clear if these products were created by re-exciting transient species within the duration of a long laser pulse. The formation of $[Fe(CN)_5OH]^{3-}$ is pH-dependent and its presence is probably only significant in alkaline solutions[9]. In a radiolysis study[47] the CN-stretch band of this species has been identified at 2102 cm^{-1}. In this spectral region no clear photoproduct band can be distinguished in our transient spectra at long time delays. Other work has assigned a peak at 2115 cm^{-1} to aquacyanoferrate(III) species[48], while the aquapentacyanoferrate(III) complex has been identified at 2120 ± 10 cm^{-1}.[15] None of these molecules could be resolved in our study.

5 Conclusions

By combining transient IR absorption with ultrafast photoelectron spectroscopy, new insight into the LMCT dynamics of aqueous ferricyanide was obtained. Thanks to the high sensitivity of PES to the oxidation state of the metal center, we were able to unequivocally establish that impulsive electron transfer to the iron takes place upon photo excitation, followed by back electron-transfer within about 0.5 ps in water. This number is fully consistent with the fastest time constant retrieved from a global fit of the transient IR spectra. The corresponding short-lived transient species formed after 400 nm excitation is characterized by an intense and strongly red-shifted CN-stretch vibration, which is reminiscent of the stronger oscillator strength and red shift of the T_{1u} CN-stretch transition of ferrocyanide with respect to ferricyanide.

The IR TA data also confirms that most of the LMCT dynamics takes place within the first picosecond after excitation, and indicates that the electron back transfer is solvent dependent (0.5 ps in water vs. 1.2 ps in Etgly). After this time, all molecules are in the electronic ground state of the ferric species, however, with significant excitation of the high-frequency CN-stretch vibration. After 265 nm excitation the electronic decay is faster and even higher levels of the CN-stretch modes are populated. A quantitative fit, based on a simple vibrational relaxation model, suggests an impulsive deformation along the C-N coordinate upon excitation and reveals a vibrational lifetime of 8 ps in H_2O, which is almost identical to the decay times measured upon direct infrared excitation of the vibrational mode.

In contrast to a previous transient IR study in DMSO and acetonitrile[14] we find no indication of photo-induced symmetry-breaking. The two IR bands associated with an ion of reduced symmetry in that work decay on clearly different timescales than in water. We re-assigned them to the anharmonically shifted $0-1$ and the $1-2$ transition of the T_{1u}-mode in a fully octahedral complex.

Our study also shows that less than 2 % of all excited molecules undergo photochemical change upon 400 nm excitation. This estimate is based on the tiny bleach remaining in the IR transient data at long delays and it is consistent with early flash photolysis experiments[9]. The photo product is identified as the aquapentacyanoferrate(II) species. This implies the dissociation of a cyanide radical, in contrast to the much more efficient ejection of a CN^- ion when the ferrous complex is excited[5–7]. The aquapentacyanoferrate(II) species is a direct product of LMCT excitation and is not formed by re-excitation of a aquapentacyanoferrate(III) intermediate, as previously suggested[8]. The final concentration of $[Fe(CN)_5OH_2]^{3-}$ appears to be higher under 265 nm excitation than under 400 nm excitation, suggesting that more efficient impulsive excitation of the CN-stretch modes is correlated with the probability for a CN radical to dissociate and escape the solvent cage.

Appendix: Model for vibrational excitation and decay

We assume that the initial population of vibrational levels $n = \{0,1,\dots\}$ follows a normalized Poisson distribution p_n. The fraction of molecules missing from the ground state, which cause the bleach signal at the fundamental frequency is thus $1-p_0$. In addition, there is another negative contribution from stimulated emission from the $v=1$ level, so the total signal at the fundamental frequency is proportional to $I_{0,1}(t) = -(1-p_0(t)) - p_1(t)$. Transitions between excited vibrational levels n and $n+1$ are composed of a positive excited state absorption proportional to the population p_n in level n and a negative stimulated emission proportional to p_{n+1}. As a result

$$I_{0,1}(t) = (p_0(t) - p_1(t)) - 1 \quad (6)$$

$$I_{n,n+1}(t) = (n+1)\,(p_n(t) - p_{n+1}(t))\ (n>0) \quad (7)$$

View Article Online
DOI: 10.1039/C7CP03337K

The factor $(n+1)$ reflects the increase in transition dipole strength with increasing quantum number of a harmonic oscillator.

The decay of the initial population is described by a sequential model

$$\frac{dp_0}{dt} = k_{1,0}p_1 \quad (8)$$

$$\frac{dp_n}{dt} = k_{n+1,n}p_{n+1} - k_{n,n-1}p_n, (n>0)$$

where only the slowest rate $k_{1,0}$ is a free parameter and

$$k_{n,n-1} = nk_{1,0} = \frac{n}{\tau_{1,0}}. \quad (9)$$

This scaling is the same as for the radiative transition dipoles and has the same perturbative origin.

The T_{1u} peak in the FTIR spectrum is best fitted by a Lorentzian while the excited state bands are more Gaussian-like. For simplicity, we assume Gaussian line shapes for all transitions

$$G_n(\nu,\nu_n,\Delta\nu_n) = \frac{1}{\sqrt{\pi}\Delta\nu_n}\exp\left[-\frac{(\nu-\nu_n)^2}{\Delta\nu_n^2}\right] \quad (10)$$

where the center frequencies are given by the fundamental transition frequency ν_0 and the anharmonicity x_a:

$$\nu_n = \nu_0 + nx_a \quad (11)$$

Likewise, we assume a monotonous increase of the band widths according to

$$\Delta\nu_n = \Delta\nu_0 + n\Delta w \quad (12)$$

The fitted spectrum is thus given by

$$S(\nu,t|\nu_0,\Delta\nu_0,x_a,\Delta w,\mu,\tau_{1,0}) = \sum_{n=0}^{n_{max}} I_{n,n+1}(t)G_n(\nu,\nu_n,\Delta\nu_n) \quad (13)$$

The position ν_0 and width $\Delta\nu_0$ of the fundamental transition, as well as the anharmonicity x_a are in principle known, but are allowed to vary slightly in the fit to account for an imperfect frequency calibration and limited resolution of the spectrometer. This leaves essentially two free parameters, the mean of the initial Poisson distribution μ and the decay time of the $v=1$ level $\tau_{1,0}$. The increase in bandwidth Δw of the order of 20 % has a moderate influence on these two values by reducing the height of peaks for large n.

Acknowledgments

The authors acknowledge funding from the Swiss NSF via the NCCR:MUST and the R'Equip contract 206021_145057.

References

1 M. Chergui, *Acc. Chem. Res.*, 2015, **48**, 801–808.
2 M. Shirom and G. Stein, *Isr. J. Chem.*, 1969, **7**, 405–412.
3 H. B. Gray and N. Beach, *J. Am. Chem. Soc.*, 1963, **85**, 2922–2927.
4 M. Shirom and G. Stein, *J. Chem. Phys.*, 1971, **55**, 3372–3378.
5 M. Shirom and G. Stein, *J. Chem. Phys.*, 1971, **55**, 3379–3382.
6 M. Reinhard, T. Penfold, F. Lima, J. Rittmann, M. Rittmann-Frank, R. Abela, I. Tavernelli, U. Rothlisberger, C. Milne and M. Chergui, *Struct. Dyn.*, 2014, **1**, 024901.
7 M. Reinhard, G. Auböck, N. A. Besley, I. P. Clark, M. W. Hanson-Heine, R. Horvath, T. S. Murphy, T. J. Penfold, M. Towrie, M. W. George and M. Chergui, *J. Am. Chem. Soc.*, accepted for publication.
8 L. Moggi, F. Bolletta, V. Balzani and F. Scandola, *J. Inorg. Nucl. Chem.*, 1966, **28**, 2589–2597.
9 M. Fuller, K. Lebrocq, E. Leslie and I. Wilson, *Aust. J. Chem.*, 1986, **39**, 1411–1419.
10 J. J. Alexander and H. B. Gray, *J. Am. Chem. Soc.*, 1968, **90**, 4260–4271.
11 R. Gale and A. J. McCaffery, *J. Chem. Soc., Dalton Trans.*, 1973, 1344–1351.
12 H. Bolvin, *J. Phys. Chem. A*, 1998, **102**, 7525–7534.
13 A. H. Upton and B. E. Williamson, *J. Phys. Chem.*, 1994, **98**, 71–76.
14 W. Zhang, M. Ji, Z. Sun and K. J. Gaffney, *J. Am. Chem. Soc.*, 2012, **134**, 2581–2588.
15 E. Herington and W. Kynaston, *J. Chem. Soc.*, 1955, 3555–3556.
16 T. L. Courtney, Z. W. Fox, K. M. Slenkamp and M. Khalil, *J. Chem. Phys.*, 2015, **143**, 154201.
17 O. Link, E. Lugovoy, K. Siefermann, Y. Liu, M. Faubel and B. Abel, *Appl. Phys. A*, 2009, **96**, 117–135.
18 O. Link, E. Vöhringer-Martinez, E. Lugovoj, Y. Liu, K. Siefermann, M. Faubel, H. Grubmüller, R. B. Gerber, Y. Miller and B. Abel, *Faraday Discussions*, 2009, **141**, 67–79.
19 K. R. Siefermann, Y. Liu, E. Lugovoy, O. Link, M. Faubel, U. Buck, B. Winter and B. Abel, *Nature chemistry*, 2010, **2**, 274–279.
20 K. Nishizawa, K. Ohshimo and T. Suzuki, *J. Chin. Chem. Soc.*, 2013, **60**, 1403–1410.
21 H. Okuyama, Y.-I. Suzuki, S. Karashima and T. Suzuki, *J. Chem. Phys.*, 2016, **145**, 074502.
22 F. Buchner, A. Lübcke, N. Heine and T. Schultz, *Rev. Sci. Instr.*, 2010, **81**, 113107.
23 A. Moguilevski, M. Wilke, G. Grell, S. Bokarev, S. Aziz, N. Engel, A. Raheem, O. Kühn, I. Y. Kiyan and E. Aziz, *ChemPhysChem*, 2016, **18**, 465–469.
24 M. Borgwardt, M. Wilke, I. Y. Kiyan and E. F. Aziz, *Phys. Chem Chem. Phys.*, 2016, **18**, 28893–28900.
25 R. Seidel, S. Thürmer, J. Moens, P. Geerlings, J. Blumberger

View Article Online
DOI: 10.1039/C7CP03337K

and B. Winter, *J. Phys. Chem. B*, 2011, **115**, 11671–11677.
26 R. Al-Obaidi, M. Wilke, M. Borgwardt, J. Metje, A. Moguilevski, N. Engel, D. Tolksdorf, A. Raheem, T. Kampen, S. Mähl *et al.*, *New J. Phys.*, 2015, **17**, 093016.
27 M. Faubel, K. Siefermann, Y. Liu and B. Abel, *Acc. Chem. Res.*, 2011, **45**, 120–130.
28 Y. El Khoury, L. J. Van Wilderen, T. Vogt, E. Winter and J. Bredenbeck, *Rev. Sci. Inst.*, 2015, **86**, 083102.
29 J. Ojeda, C. Arrell, J. Grilj, F. Frassetto, L. Mewes, H. Zhang, F. van Mourik, L. Poletto and M. Chergui, *Struct. Dyn.*, 2016, **3**, 023602.
30 C. Arrell, J. Ojeda, M. Sabbar, W. Okell, T. Witting, T. Siegel, Z. Diveki, S. Hutchinson, L. Gallmann, U. Keller, F. van Mourik, R. T. Chapman, C. Cacho, N. Rodrigues, I. C. E. Turcu, J. W. G. Tisch, E. Springate, J. P. Marangos and M. Chergui, *Rev. Sci. Inst.*, 2014, **85**, 103117.
31 C. Arrell, J. Ojeda, L. Mewes, J. Grilj, F. Frassetto, L. Poletto, F. Van Mourik and M. Chergui, *Phys. Rev. Lett.*, 2016, **117**, 143001.
32 J. A. N. Friend and W. N. Smirles, *J. Chem. Soc. (Resumed)*, 1928, 2242–2245.
33 Y.-I. Suzuki, K. Nishizawa, N. Kurahashi and T. Suzuki, *Phys. Rev. E*, 2014, **90**, 010302.
34 G. Prampolini, P. Yu, S. Pizzanelli, I. Cacelli, F. Yang, J. Zhao and J. Wang, *J. Phys. Chem. B*, 2014, **118**, 14899–14912.
35 M. L. Moyá and A. Rodríguez, *Transition Met. Chem.*, 1991, **16**, 230–235.
36 G. M. Sando, Q. Zhong and J. Owrutsky, *J. Chem. Phys.*, 2004, **121**, 2158–2168.
37 P. Yu, F. Yang, J. Zhao and J. Wang, *J. Phys. Chem. B*, 2014, **118**, 3104–3114.
38 P. Hamm, S. Ohline and W. Zinth, *J. Chem. Phys.*, 1997, **106**, 519–529.
39 V. Botan and P. Hamm, *J. Chem. Phys.*, 2008, **129**, 164506.
40 C. Ventalon, J. M. Fraser, M. H. Vos, A. Alexandrou, J.-L. Martin and M. Joffre, *Proc. Natl. Acad. Sci. U. S. A.*, 2004, **101**, 13216–13220.
41 M. S. Lynch, B. E. Van Kuiken, S. L. Daifuku and M. Khalil, *J. Phys. Chem. Lett.*, 2011, **2**, 2252–2257.
42 E. Pomarico, M. Silatani, F. Messina, O. Bräm, A. Cannizzo, E. Barranoff, J. H. Klein, C. Lambert and M. Chergui, *J. Phys. Chem. C*, 2016, **120**, 16459–16469.
43 N. Engel, S. I. Bokarev, A. Moguilevski, A. A. Raheem, R. Al-Obaidi, T. Möhle, G. Grell, K. R. Siefermann, B. Abel, S. G. Aziz, O. Kühn, M. Borgwardt, I. Y. Kiyan and E. F. Aziz, *Phys. Chem. Chem. Phys*, 2017, **19**, 14248–14255.
44 D. E. Milligan and M. E. Jacox, *J. Chem. Phys.*, 1967, **47**, 278.
45 P. Coulter, M. P. Grubb, D. Koyama, I. V. Sazanovich, G. M. Greetham and A. J. Orr-Ewing, *J. Phys. Chem. A*, 2015, **119**, 12911–12923.
46 C. A. Rivera, N. Winter, R. V. Harper, I. Benjamin and S. E. Bradforth, *Phys. Chem. Chem. Phys.*, 2011, **13**, 8269–83.
47 S. Le Caër, G. Vigneron, J. Renault and S. Pommeret, *Radiat. Phys. Chem.*, 2007, **76**, 1280–1284.
48 M. G. de Oliveira, J. Langley *et al.*, *J. Chem. Soc., Dalton Trans.*, 1995, 2013–2019.